International Journal of
MATERIALS RESEARCH

Zeitschrift für METALLKUNDE

Original Contributions

Katharina Esleben[a], Bronislava Gorr[a], Hans-Jürgen Christ[a], Christian Pritzel[b], Debashis Mukherji[c], Joachim Rösler[c], Přemysl Beran[d,e], Pavel Strunz[d], Markus Hoelzel[f], Ralph Gilles[f]

[a] Institut für Werkstofftechnik, Universität Siegen, Siegen, Germany
[b] Institut für Bau- und Werkstoffchemie, Universität Siegen, Siegen, Germany
[c] Institut für Werkstoffe, TU Braunschweig, Braunschweig, Germany
[d] Nuclear Physics Institute of the CAS, Řež, Czech Republic
[e] ESS (European Spallation Source ERIC), Lund, Sweden
[f] Heinz Maier-Leibnitz Zentrum (MLZ), TU München, Garching, Germany

Effect of Cr and Ni on the microstructural evolution in Co–Re–Cr–Ni alloys

The present study focuses on the microstructural evolution in Co–Re–Cr–Ni alloys at high temperatures. Four alloys with different Cr and Ni contents were studied. The microstructural examinations were performed using complementary methods of scanning electron microscopy, transmission electron microscopy, differential scanning calorimetry and neutron diffraction. Based on the experimental results and assisted by thermodynamic calculations, the effect of Cr and Ni on the microstructure could be identified. While both Ni and Cr, but Cr only if Ni is also present in the alloy, stabilize the fcc phase, the impacts of these elements on the σ phase formation are different. It was found that the temperature stability of the σ phase enhances with increasing Cr content, whereas Ni reduces the required Cr concentration for the σ phase formation. The evaluation of the Cr and Ni effects on the microstructural evolution contributes to a fundamental understanding of the alloy behaviour and, thus, is a key aspect for successful alloy development.

Keywords: Cr effect; Ni effect; Co–Re-based alloys; Microstructure evolution; Phase stability

1. Introduction

Numerous studies have reported on the positive effect of refractory element additions to high-temperature materials. These additions primarily aim at the improvement of alloy mechanical properties, particularly creep resistance [1–3]. Despite relatively high cost, Re additions are common in modern high-temperature materials for its high strengthening effect. However, Re also belongs to the elements which exhibit a high potential for forming topologically close-packed phases which are inherently brittle. Therefore, the concentration of Re must be chosen very carefully. The third generation of single crystal Ni-base alloys contains Re additions of 5–6 wt.% [3–5]. New high-temperature materials with a high amount of Re, namely Co–Re-base alloys, have been developed to exploit the exceptional strengthening potential of this element and therefore to design a microstructure which is beneficial for high-temperature applications [6–8]. The complete miscibility of Re in Co yields a unique property combination required for high-temperature applications as the Co–Re matrix combines both strength and ductility. The strength of the Co–Re alloys can be sensitively enhanced with increased Re content. Furthermore, this alloy class substantially benefits from the refractory element addition as Re increases the alloy melting point allowing potentially higher application temperatures which exceed those of Ni-base superalloys [6].

The binary hcp-single phase Co-17Re alloy (all composition values are given in at.%) was found to be inherently ductile and to show prospects in terms of high-temperature strength, but it does not possess reliable oxidation resistance because of the evaporation of Re-oxides [7, 9]. Cr was added

to the binary alloy Co-17Re to improve high-temperature corrosion resistance. This Cr addition also causes the formation of coarse particles of the topologically close-packed σ phase (Cr_2Re_3) which imparts strengthening due to its high hardness but also adversely affects ductility [9, 10]. It was found that a decrease of the volume fraction of the brittle σ phase can be realized by adding Ni to the Co-17Re-23Cr alloy if the samples are quenched after solution treatment. Another beneficial effect of Ni is the improvement of the oxidation behaviour because of the fast formation of a protective chromia layer [11, 12]. Earlier studies revealed that Ni stabilizes the face-centred cubic (fcc) crystal structure. But it was found that with increasing volume fraction of the fcc phase the oxidation resistance of the alloy Co-17Re-23Cr-25Ni deteriorates [12]. So it was concluded that Ni has a very complex effect on the microstructure and an ambiguous impact on the high-temperature properties of the Co–Re–Cr alloy system. Furthermore, Ni and Cr seem to display a complex interacting effect that is not properly understood so far. Therefore, alloys with varying Cr and Ni concentrations have to be investigated. At present, the microstructural evolution of Co–Re–Cr–Ni alloys has only been studied in [13, 14]. While the neutron diffraction data for only one Co–Re–Cr–Ni alloy is published in [13], the microstructures of different Co–Re–Cr–Ni alloys after various heat-treatments were studied in [14], but only specifically chosen temperatures were investigated and the results were affected by martensitic transformations during cooling.

The present study deals with the experimental investigation of the microstructural evolution of Co–Re–Cr–Ni alloys with different Cr (18 at.% and 23 at.%) and Ni (15 at.% and 25 at.%) concentrations during high-temperature exposure. Different experimental techniques in combination with thermodynamic calculations were applied to understand the underlying mechanisms of the microstructural evolution. In this paper, thermodynamic calculations were performed using the specifically derived thermodynamic database. A commercial database which includes the elements Co, Re, Cr, O was used as the basis and critically edited due to inadequate results. Furthermore, the database was extended to include the element Ni. Since only limited thermodynamic data exist in the literature so far, because thermodynamic properties of the alloy systems investigated have scarcely been determined, the results of the experimental studies obtained in this study simultaneously served to adapt and improve the database by means of experimental validation of the results of the thermodynamic calculations performed.

2. Materials and experimental procedure

In this study, the microstructures of four Co–Re–Cr–Ni alloys with different Cr (18 at.% and 23 at.%) and Ni contents (15 at.% and 25 at.%) are dealt with. All alloys were produced by arc melting in a vacuum furnace and cast into bars. Afterwards, they were homogenized in a three-step solution heat-treatment (1 350 °C 5 h/1 400 °C 5 h/1 450 °C 5 h) and quenched by argon.

After homogenization and quenching, the microstructure was investigated using scanning electron microscopy (SEM) in combination with electron backscatter diffraction (EBSD) carried out on an FEI Helios Nanolab 600 equipped with an EDAX/TSL 3D EBSD system. Samples with dimensions of $10 \times 10 \times 2$ mm^3 were cut from the alloy bars, ground with SiC paper and polished using a SiO_2 polishing suspension with a size of 0.05 µm. The evolution of the microstructure at high-temperatures was examined using in-situ neutron diffraction (ND) as well as differential scanning calorimetry (DSC) additional to standard SEM technique. To correlate a specific phase transformation with particular signals in the DSC curves, additional heat-treatment tests were carried out. The corresponding samples were heated in the DSC device up to the relevant temperatures, quenched and examined via SEM. For the differential scanning calorimetry, samples with dimensions of about $3 \times 3 \times 1$ mm^3 were used. The thermal analysis was carried out in a Netzsch STA 449 C at a heating rate of 5 K min^{-1} under flowing purified argon atmosphere (625 ml min^{-1}) in Al_2O_3 crucibles. In-situ neutron diffraction measurements were performed for the two alloys containing 23 at.% Cr at Forschungs-Neutronenquelle Heinz Maier-Leibnitz (FRM II), Garching, using the instrument SPODI [15] equipped with a high-temperature furnance for in-situ studies on Co–Re alloys at elevated temperatures. The data were recorded at RT before and after the in-situ thermal cycle and at selected temperatures up to 1 450 °C using a neutron wavelength of 0.1 548 nm [13]. Transmission electron microscopy (TEM) was also performed on these two alloys (Co-17Re-23Cr-15Ni and Co-17Re-23Cr-25Ni) using an FEI Talos F200A operated at an acceleration voltage of 200 keV. Scanning transmission electron microscopy (STEM) was conducted at a camera length of 210 mm and energy-dispersive X-ray spectroscopy (EDXS) was carried out using a SuperX-detector without standards. One measurement was carried out for each phase. The TEM sample preparation was done by using the Focused Ion Beam Technology at an FEI Helios Nanolab 600. Further TEM specimens were prepared by stamping out disks of 3 mm from ground samples with a thickness of 0.1 mm. With electrochemical thinning (double-jet electropolishing, solution: 90 % acetic acid, 10 % perchloric acid, 10 V, 15 °C) thin TEM foils were produced.

3. Results and discussion

3.1. Microstructure after solution annealing

Figure 1 shows the microstructures of the alloys after homogenization and argon quenching. It is remarkable that both alloys with 23 at.% Cr exhibit lamellar precipitates of the σ phase (Cr_2Re_3) along the grain boundaries whereas in the alloys with a lower Cr concentration (18 at.%) nearly no σ phase was found after homogenization. Earlier investigations showed that the Co-17Re-23Cr-*X*Ni alloys (X = 8, 15, 25 at.%) exhibit drastically reduced volume fractions of the σ phase as compared to the Ni-free alloy Co-17Re-23Cr [12]. This finding was explained by the influence of the non-equilibrium state after argon quenching. Figure 2a shows the volume fractions of all the phases determined by ND after argon quenching (full symbols). Argon quenching supresses the formation of the σ phase. As a consequence, more Re (hcp-stabilizing element) is present in the matrix. Therefore, hcp is present as only matrix phase at RT after argon quenching for alloys containing up to 15 at.% Ni, even though there is the fcc-stabilizing effect of Ni. Nevertheless, σ forms on subsequent heating above 900 °C and remains in the alloy after slow cooling as can be seen in Fig. 2a (open symbols). This state is much nearer to equilibrium than the state after argon quenching. As can be seen in Fig. 2a, there is an increasing amount of σ phase with increasing Ni content.

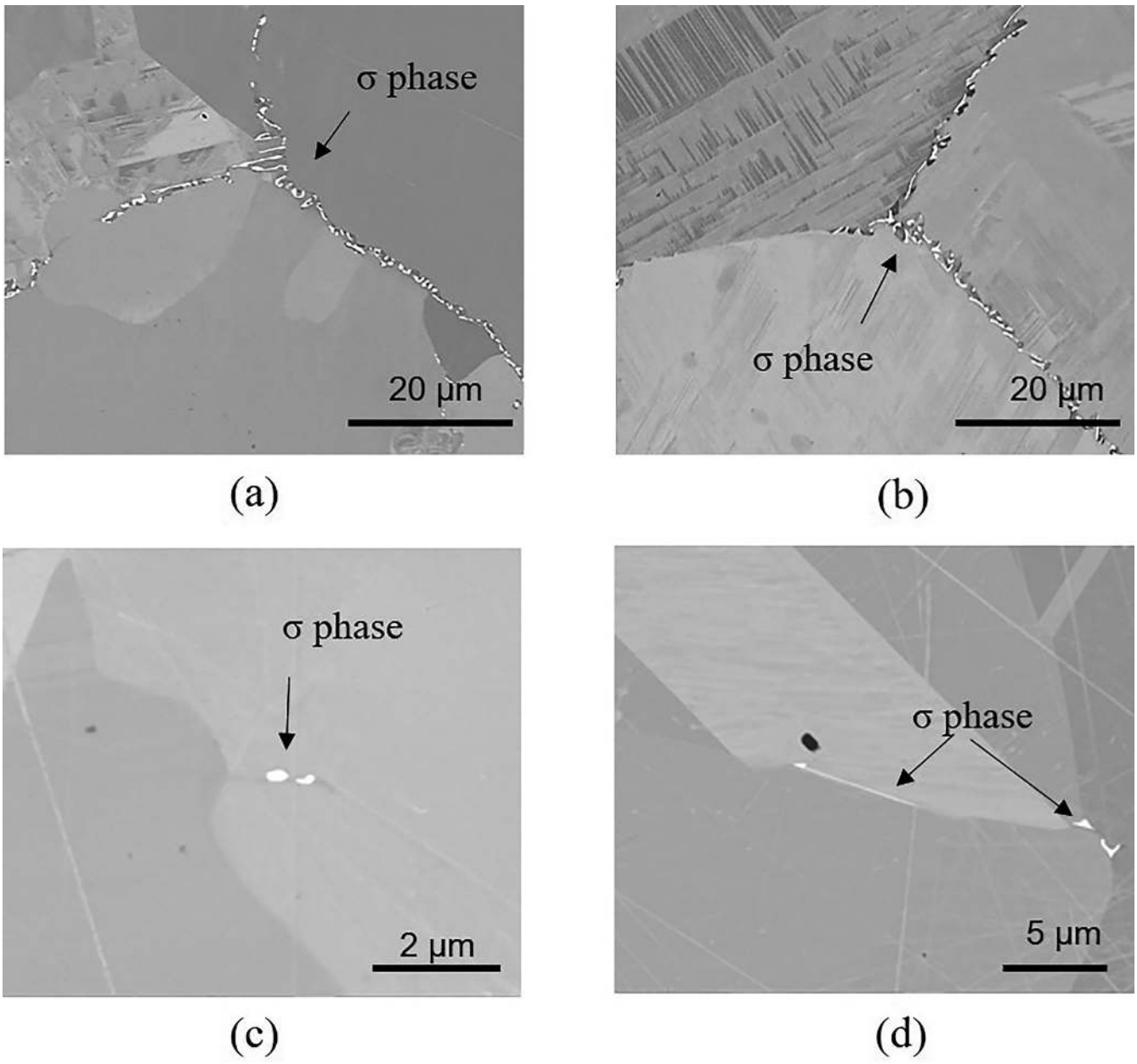

Fig. 1. SEM images obtained by the BSE detector of the alloys after solution heat treatment and argon quenching: (a) Co-17Re-23Cr-15Ni; (b) Co-17Re-23Cr-25Ni; (c) Co-17Re-18Cr-15Ni; and (d) Co-17Re-18Cr-25Ni.

A typical neutron diffractogram at RT after in-situ thermal cycle heating up to 1 450 °C is shown in Fig. 2b. The phases of fcc, hcp and σ are marked and the fits (solid lines) and measured data (crosses) as well as the difference (blue line) of both are plotted. The Rietveld refinement was performed with the FullProf program [16].

To identify the crystal structure of the alloy matrix EBSD analysis was performed in addition to ND after argon quenching. The corresponding results are shown in Table 1. The results are in line with the ND measurements: The alloys with an Ni content of 15 at.% consist of a single hexagonal close-packed (hcp) matrix whereas the alloys with a higher Ni concentration (25 at.%), additionally contain a fcc phase. It is obvious that with increasing Ni content the formation of the fcc phase is favoured.

For more precise information on the σ phase composition, TEM examination was performed on the two Co-17Re-23Cr-*X*Ni alloys with different Ni contents. Figure 3 shows TEM HAADF images of the microstructure of both alloys and the corresponding EDXS mappings. The experimentally measured compositions of the σ phase areas in comparison to the matrix areas marked in Fig. 3a and b are given in Table 2. The results show that besides Cr and Re the σ phase can solve a substantial amount of Co and Ni. Compared to the matrix, however, it is depleted in Co and Ni while enriched in Cr and Re. The σ phase in the alloy with a Ni content of 25 at.% contains only a marginally higher amount of Ni than in the alloy with a lower Ni concentration. But a higher amount of Co solved in the σ phase can be found in the alloy with an Ni content of 15 at.%. Furthermore, small zones enriched in Ni and Co which are located next to the σ phase particles can be observed in the EDXS mappings in the microstructure of both alloys. For the alloy Co-17Re-23Cr-25Ni, electron

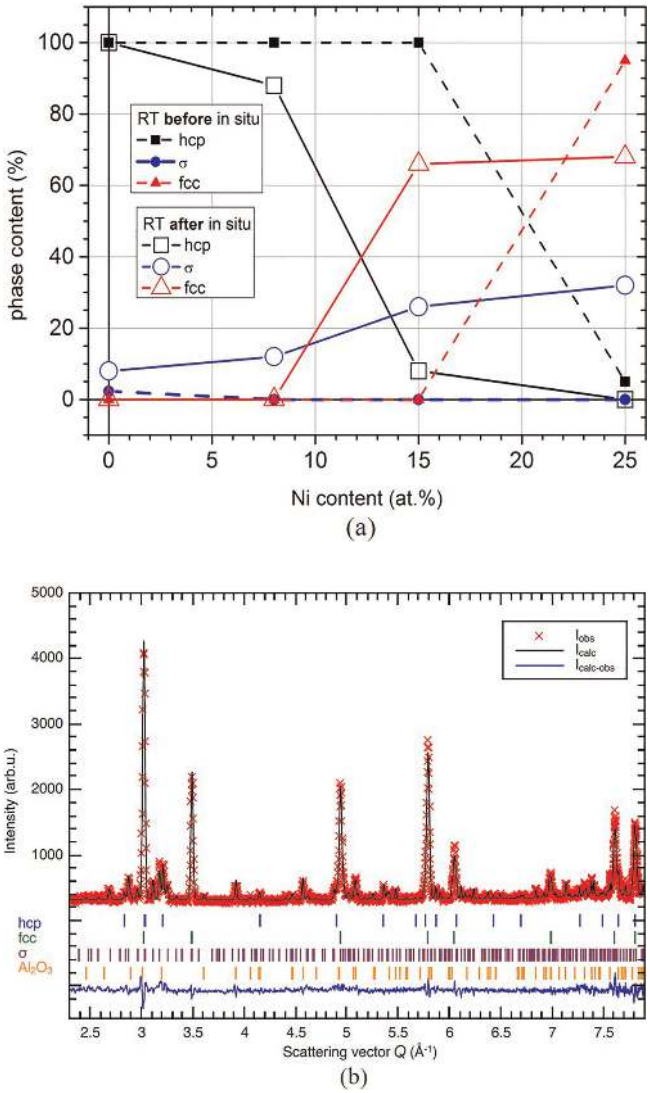

Fig. 2. (a) Phase fractions of Co-17Re-23Cr-XNi at RT as a function of the Ni content after homogenization and argon quenching (full symbols) and after in-situ thermal cycle (i.e. after slow cooling) (open symbols) determined using neutron diffraction, and (b) neutron diffractogram of Co-17Re-23Cr-15Ni at RT after in-situ thermal cycle heating up to 1 450 °C. All phases as fcc, hcp and σ are present. The Al_2O_3 peaks belong to the sample holder which was a little bit illuminated with neutrons.

diffraction analysis was performed on this Co-, Ni-enriched area. Figure 3c shows the corresponding electron diffraction pattern recorded for the area circular marked in Fig. 3b. The matrix in the vicinity of the σ phase is obviously the γ Co-based phase.

3.2. Microstructure evolution during high-temperature exposure

The microstructural evolution during high-temperature exposure was examined using different experimental methods. DSC thermal analysis is an appropriate tool for analysing solid–solid phase transformations [17]. To attribute the signals in the heating curves to the occurring phase transitions, the peak appearance (endothermic or exothermic) of the particular transformation must be known. If

Table 1. Phase composition of the matrix of the alloys studied after homogenization and argon quenching (determined by EBSD).

Alloy	Matrix
Co-17Re-23Cr-15Ni	hcp (ε)
Co-17Re-23Cr-25Ni	hcp (ε) + fcc (γ)
Co-17Re-18Cr-15Ni	hcp (ε)
Co-17Re-18Cr-25Ni	hcp (ε) + fcc (γ)

various phase transitions occur during heating, additional experimental methods are necessary to distinguish and identify the processes and correlate these results with the signals from the DSC measurements [18]. The σ phase formation and dissolution in $Al_xCoCrFeNi$ and $AlCrFeNiMo_{0.2}$ high entropy alloys as well as the ε → γ transformation in Co–Ni alloys are detected as endothermic reactions in DSC heating curves. Ab-initio calculations by Palumbo et al. reveal positive formation enthalpies of the σ phase for the binary Cr–Re system [19]. According to these references [19 – 21], it can be assumed that all transformations in the Co–Re–Cr–Ni alloy system are of endothermic nature during heating. The fact that the σ phase formation and dissolution have been detected as endothermic reactions during heating obviously results from the simultaneously occurring transformations in the surrounding matrix. In other words, if the σ phase dissolves, the alloy matrix does not transform back to the original solid solution but undergoes its own phase transformation. So, all phase transitions are endothermic and it is not possible to separate the processes due to the peak shape in the DSC curves. Therefore, results of the DSC thermal analysis were complemented by phase analyses by means of SEM as well as applying neutron diffraction.

Ni effect

The DSC heating curves for alloys Co-17Re-23Cr-15Ni and Co-17Re-23Cr-25Ni in the temperature range 720 – 1 350 °C appear to be very similar. Figure 4a shows illustratively the DSC heating curve for the alloy Co-17Re-23Cr-15Ni. The corresponding peak temperatures of the alloy Co-17Re-23Cr-25Ni are listed in Table 3. As described above, additional samples of the alloy Co-17Re-23Cr-15Ni were heated up to 850 °C, 1 075 °C and 1 200 °C and then quenched to freeze the alloy microstructure. The results of the microstructural analyses of these samples are shown in Fig. 4b–d. The results of neutron diffraction investigations are summarized in Fig. 5. It is apparent that both DSC measurements show four endothermic peaks. The small endothermic peak at 836 °C in the DSC curve of the Co-17Re-23Cr-15Ni alloy indicates the beginning of the σ phase formation at grain boundaries (see Fig. 4b). With increasing temperature, two other endothermic peaks appear at 1 057 and 1 081 °C. Figure 4c reveals that the volume fraction of the σ phase is strongly increased by heating up the alloy to 1 075 °C. Also the ND results show an increasing volume fraction of the σ phase during heating (compare Figs. 2a and 5a). Furthermore, the neutron diffraction results reveal that at temperatures ≥1 100 °C the precipitation of the σ phase is accompanied by the ε → γ transformation because of enhanced volume fractions of

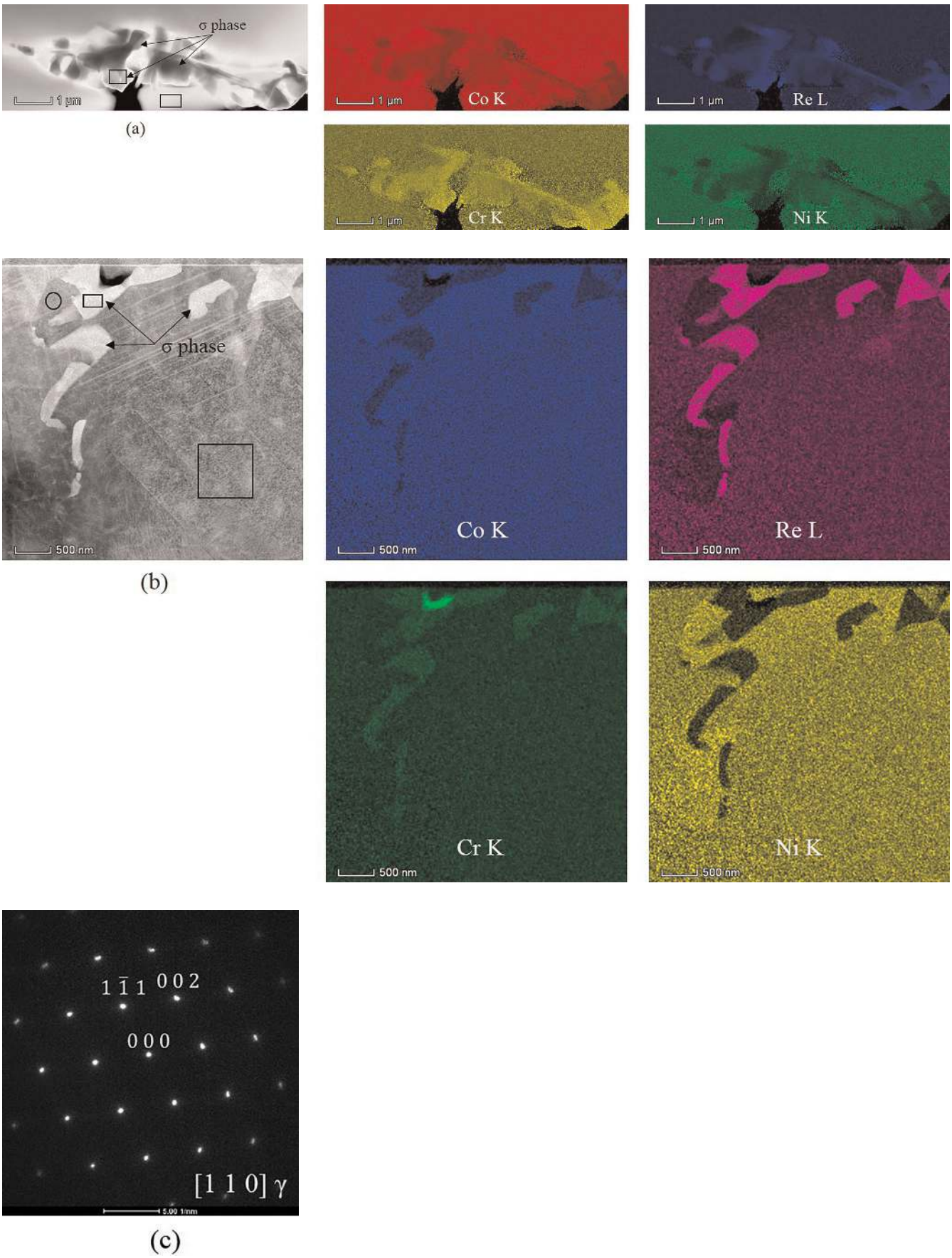

Fig. 3. TEM HAADF images (the rectangular label marks the σ phase areas used for EDXS quantification) and element distribution maps of the alloys after solution heat treatment: (a) Co-17Re-23Cr-15Ni; (b) Co-17Re-23Cr-25Ni; and (c) selected area diffraction pattern along the [110] zone axis of the γ phase from the position circular labelled in (b).

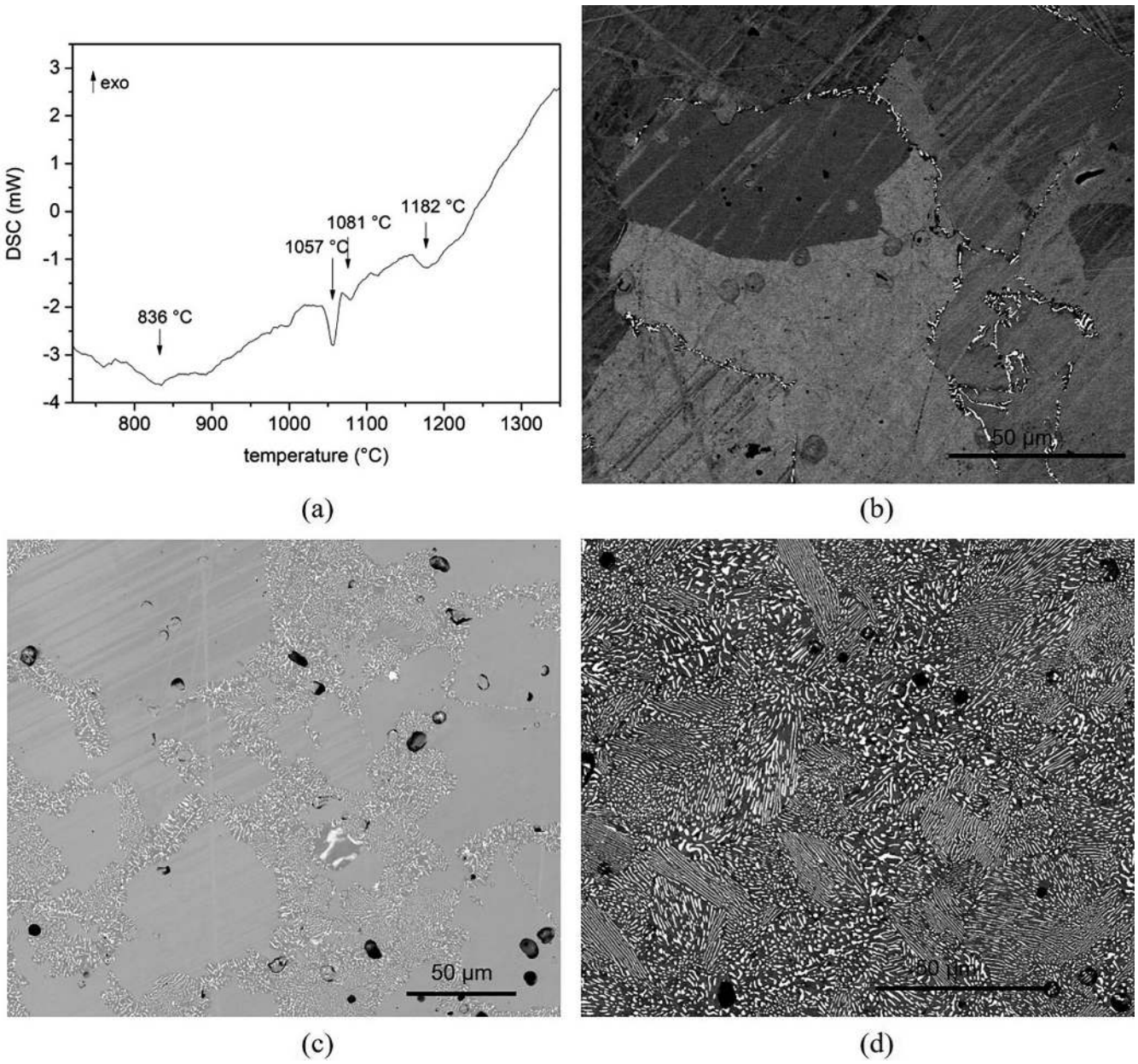

Fig. 4. (a) DSC heating curve (heating rate 5 K min^{-1}) of the Co-17Re-23Cr-15Ni alloy and SEM images obtained by the BSE detector of the alloy Co-17Re-23Cr-15Ni heated up to (b) 850 °C, (c) 1 075 °C, and (d) 1 200 °C.

both fcc and σ phases. It is highly probably that such a correlated process of $\varepsilon \rightarrow \sigma + \gamma$ will also take place at lower temperatures as assumed in the extrapolation of the ND results. EBSD analysis was performed to prove this hypothesis. The EBSD phase map in Fig. 6 shows exemplarily the microstructure of the Co-17Re-23Cr-15Ni alloy after a heat treatment for 2 h at 1 000 °C. The σ phase precipitates at the grain boundaries and there are small areas consisting of the γ phase next to the σ phase. Despite different heat treatment conditions of the samples in the DSC (continuous heating-up) and used for the EBSD analysis (isothermal heating), Fig. 6 proves that the cellular precipitation process with the sequence $\varepsilon \rightarrow \sigma + \gamma$ also takes place at lower temperatures as assumed above. So, it can be assumed that the first endothermic reaction of the alloy with 15 at.% Ni is also a correlated process of the σ phase formation and $\varepsilon \rightarrow \gamma$ transformation. The other two peaks in the DSC measurement correspond to the proceeding σ phase and fcc formation. At 1 182 °C another broad peak occurred. Figures 4d and 5a demonstrate that at around 1 200 °C a lot of σ phase is precipitated and the matrix is completely transformed into the fcc phase. The fact that the precipitation process evokes several signals during heating can be attributed to the different precipitation locations. At low temperatures, the favoured nucleation at grain boundaries was observed (see Fig. 4b). At higher temperatures, the σ phase reaction front expands in the grain interiors (see Fig. 4d). The different nucleation sites apparently require different energies and the introduction of cellular reaction fronts as additional interfaces provides additional energies to form the σ phase. Besides, the surface energies as well as the kinetic aspects of the growing particles lead to additional signals. Such an effect was also observed by Milkereit et al. [22]. Furthermore, the simultaneously occurring $\varepsilon \rightarrow \gamma$

Table 2. Measured composition (in at.%) of the marked areas of the σ phase and matrix phase (rectangular labels see Fig. 2) in the alloys Co-17Re-23Cr-15Ni and Co-17Re-23Cr-25Ni after homogenization and argon quenching.

Alloy	Phase	Co	Re	Cr	Ni
Co-17Re-23Cr-15Ni	σ	34.80	29.01	29.06	7.13
Co-17Re-23Cr-25Ni	σ	24.60	35.41	31.13	8.86
Co-17Re-23Cr-15Ni	matrix	48.56	14.85	21.05	15.53
Co-17Re-23Cr-25Ni	matrix	38.29	15.58	20.81	25.32

Table 3. Measured peak temperatures in the DSC heating curves (heating rate 5 K min^{-1}) of Co-17Re-23Cr-25Ni and Co-17Re-18Cr-25Ni.

Alloy	Co-17Re-23Cr-25Ni	Co-17Re-18Cr-25Ni
Peak 1	903 °C	892 °C
Peak 2	1 056 °C	1 057 °C
Peak 3	1 080 °C	1 081 °C
Peak 4	1 261 °C	1 114 °C

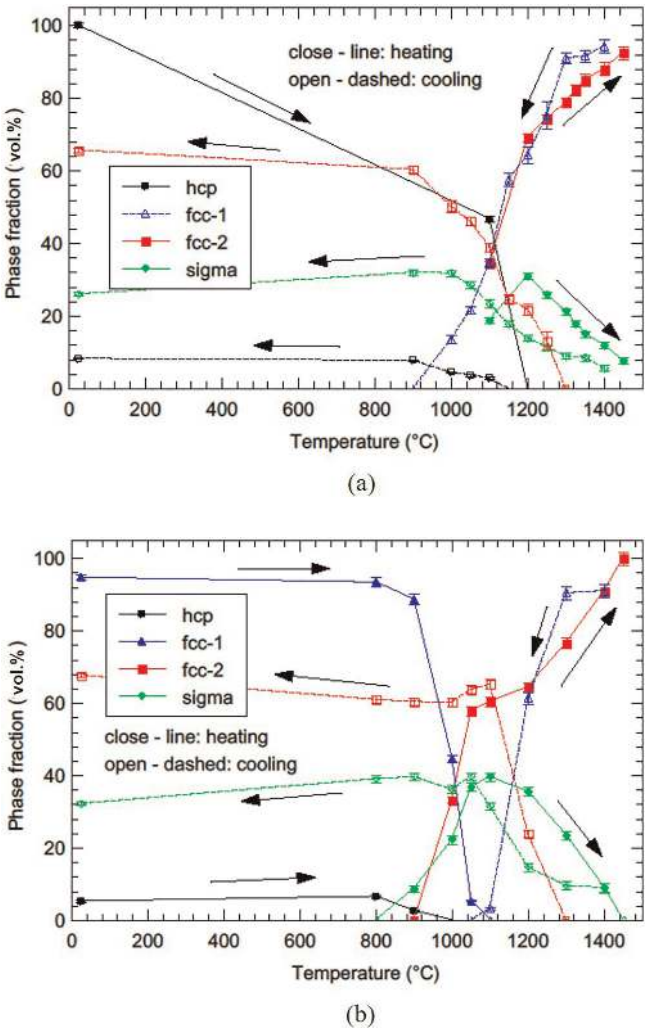

Fig. 5. Changes in the phase fractions during heating and cooling determined from the neutron diffraction results (a) Co-17Re-23Cr-15Ni, and (b) Co-17Re-23Cr-25Ni.

transformation also contributes to the appearance of various DSC signals.

The DSC curve of the alloy Co-17Re-23Cr-25Ni exhibits peaks at similar temperatures. From the ND results (see Fig. 5b) it can be deduced that the peak at 903 °C corresponds to the beginning of the σ phase formation (predominantly at grain boundaries). Which kind of matrix transformation goes along with this σ precipitation cannot be derived from the ND measurements. The following two peaks belong to the proceeding σ phase precipitation and the simultaneously occurring formation of a new fcc matrix phase (denoted as fcc-2). As the σ phase is mostly composed of Re, Cr and Co, the fcc-2 phase with a smaller lattice parameter forms because of the formation of the σ phase and the correspondingly reducing amount of solved Cr and Re in the matrix. From the ND data it becomes clear that a significant amount of the fcc-2 and σ phases has formed by reaching a temperature of 1 000 °C. So, it is assumed that the occurrence of the two successive peaks (1 056/1 080 °C) results from the cellular reaction: fcc-1 → σ + fcc-2. For the Co–Re system no information about the intensity of precipitation reactions or about the precipitated volume fraction required to cause a signal in the DSC curve exists. From the ND data it can be derived that a change of about 10 vol.% of σ phase manifests itself in the formation of a new peak in the DSC curve. The last low and broad peak at 1 261 °C is a result of the beginning σ phase dissolution which is also reflected in Fig. 5a and b. The dissolution of the σ phase causes a rearrangement of atoms in the newly formed fcc-2 matrix phase, particularly due to the higher amount of Re which is released from the dissolution of the σ phase. This process apparently requires additional energy and is therefore expressed as an endothermic reaction.

In pure Co, the $\varepsilon \leftrightarrow \gamma$ phase transformation is a diffusionless martensitic process as it occurs abruptly [19, 23]. In contrast, in the Ni-containing Co-17Re-23Cr alloys this phase transformation can take place martensitically [14] but it can also be a diffusion-controlled process as higher

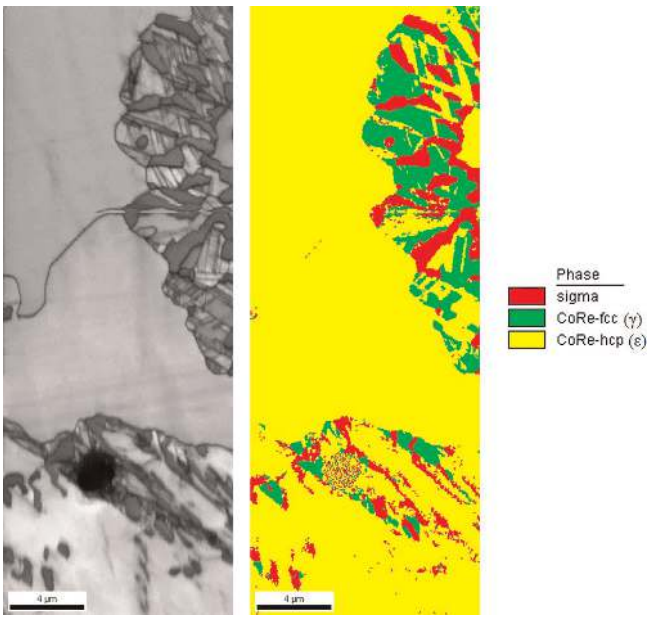

Fig. 6. EBSD analysis of the microstructure of Co-17Re-23Cr-15Ni after 2 h exposure at 1 000 °C.

temperatures are involved. Diffusion-controlled phase transformations are typical for many alloys, e. g. stainless steels [24–26]. In addition to the matrix transformation, the precipitation of the σ phase in Cr-rich steels is possible which usually causes element partitioning in the ferrite matrix. The resulting decrease in the Cr content and the following increase in the Ni concentration in the surrounding matrix lead to the formation of an austenite phase (γ) [24, 26, 27]. A similar co-existence of the two matrix phases, i. e. ε and γ, is observed in the Co-17Re-23Cr-15Ni alloy (see Fig. 6). This local formation of the fcc phase and the σ phase seems to occur linked and simultaneously as a result of a discontinuous reaction starting from the grain boundaries. Microstructural examinations of the Ni-free Co-17Re-23Cr alloy showed that σ phase formation occurs in a wide temperature range at which the fcc phase is not yet stable. ND results revealed that in the Ni-free alloys the $\varepsilon \leftrightarrow \gamma$ phase transformation does not start before 1 300 °C [28, 29]. Based on these results one can assume that the formation of the σ phase provokes a local depletion in Re and Cr and enrichment in Co and Ni in the surrounding area of the σ phase. As Re stabilizes the hcp phase while Ni stabilizes the fcc phase and decreases the $\varepsilon \leftrightarrow \gamma$ transformation temperature, this change in chemical composition supports the local transformation of ε-Co to γ-Co. According to Fig. 6, the matrix between the σ phase does not entirely consist of fcc phase. Instead hcp phase is also observed. This is probably due to a transformation from fcc to hcp upon cooling from 1 000 °C to ambient temperature.

In the case of the Co-17Re-23Cr-25Ni alloy, the matrix already contains mostly fcc phase after homogenization and quenching (see Figs. 2a and 5b). So, in this alloy the discontinuous precipitation character of the σ phase provokes the formation of the fcc-2 matrix phase during heating with a smaller lattice parameter due to the reduced concentration of Re and Cr.

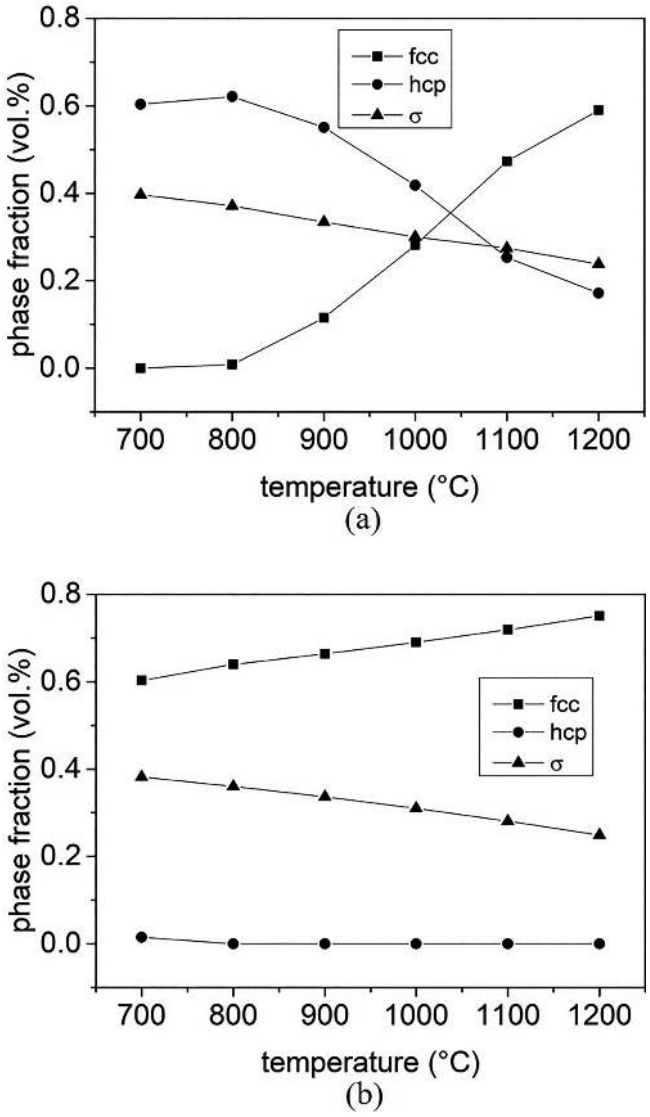

Fig. 7. Thermodynamic calculations of the phase fractions of the different phases in the temperature range of 700–1 200 °C in alloy (a) Co-17Re-23Cr-15Ni, and (b) Co-17Re-23Cr-25Ni using the software FactSage.

For further information about the phase stabilities in the Co–Re–Cr–Ni system, thermodynamic calculations were carried out. The unerring assessment of the stability of the different phases is a valuable means to understand the thermodynamic driving forces for the phase transformations in the alloys investigated. Hence, the volume fractions of the fcc-, hcp- and σ phase in the temperature range 700 – 1 200 °C were calculated using the software FactSage. The results are plotted in Fig. 7. It becomes apparent that the fcc phase is stable over the whole temperature range of 700 – 1 200 °C for the alloy with 25 at.% Ni. Regarding the alloy with 15 at.% Ni, the fcc phase starts to form at 800 °C and becomes more stable at higher temperatures. This clearly shows the very strong stabilization effect of Ni on the fcc phase as the $\varepsilon \leftrightarrow \gamma$ phase transformation is shifted to lower temperatures. The calculations for Co-17Re-23Cr-15Ni show that the σ phase is already stable at low temperatures at which no fcc phase exists which is similar to the Ni-free Co-17Re-23Cr alloy [29]. However, the $\varepsilon \leftrightarrow \gamma$ phase transformation starts at lower temperatures compared to the Ni-

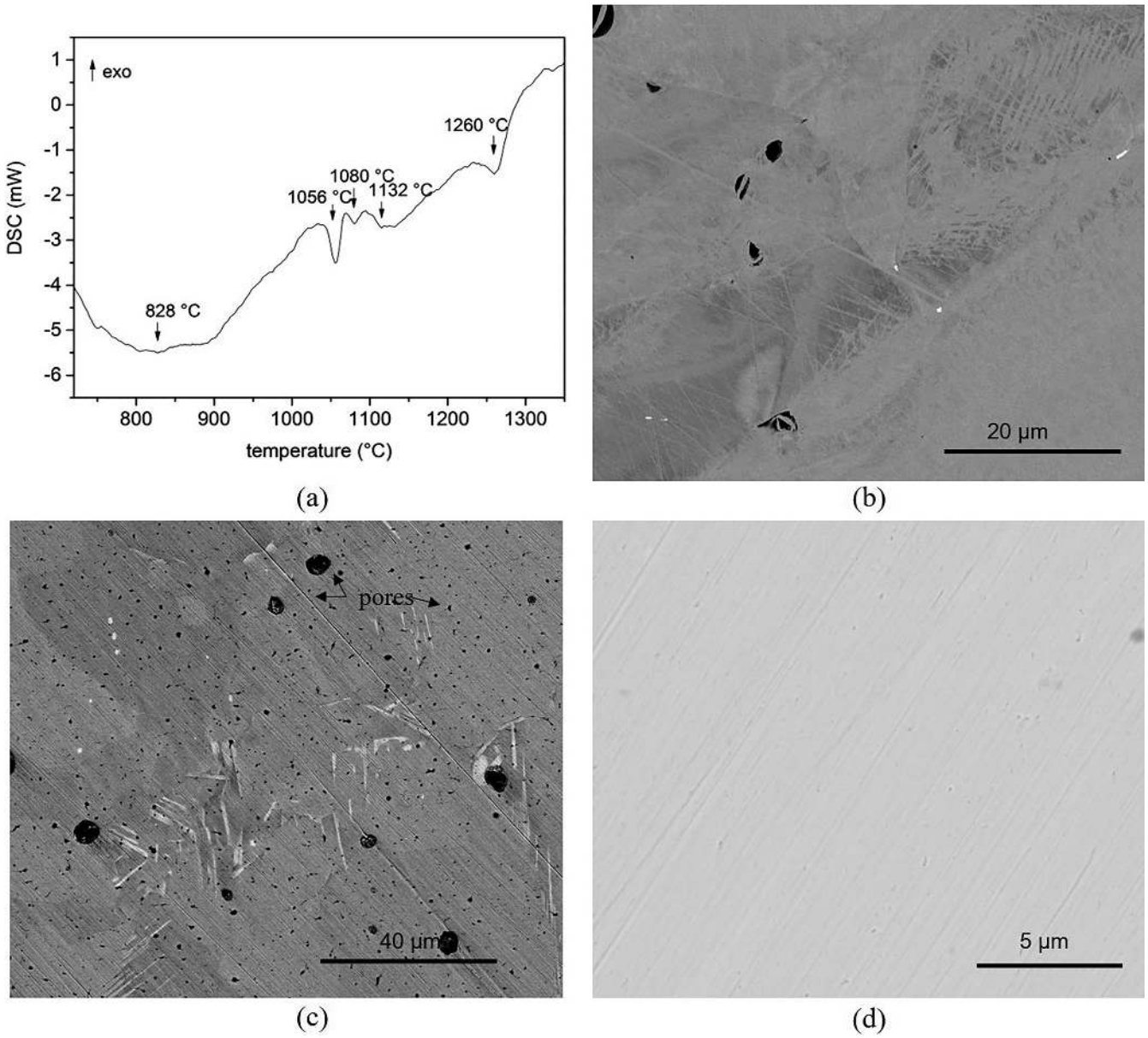

Fig. 8. (a) DSC heating curve (heating rate 5 K min^{-1}) of the Co-17Re-18Cr-15Ni alloy and SEM images obtained by the BSE detector of the alloy Co-17Re-18Cr-15Ni heated up to (b) 1 040 °C (initial formation of σ phase), (c) 1 100 °C (fine, needle-like σ particles), and (d) 1 300 °C (homogeneous matrix).

free alloy which can clearly be accounted for Ni additions. It can therefore be concluded that the σ phase precipitates and the correlated $\varepsilon \rightarrow \gamma$ transformation in the Co-17Re-23Cr-15Ni alloy or rather the formation of a new fcc-2 matrix phase in the Co-17Re-23Cr-25Ni alloy, thus, can be considered as a simultaneous process which is supported by the local Re and Cr depletion as well as Co and Ni enrichment as soon as enough σ phase has formed, as was described in our assumption above. Such an enrichment in Co and Ni next to the σ phase was proved by TEM analysis (see Fig. 3).

Cr effect

Figure 8a shows the DSC heating curve of the Co-17Re-18Cr-15Ni alloy which is to some extent different from that shown in Fig. 4a. As the DSC results of the Co-17Re-18Cr-25Ni alloy are very similar to those of the 15 at.% Ni alloy with the same Cr concentration, the DSC curve of the alloy with 25 at.% Ni is not shown here. The corresponding peak temperatures are summarized in Table 3. In the BSE micrographs of additional samples which were heated up to 1 040 °C and 1 100 °C (Fig. 8b and c), the formation of σ phase lamellae is visible. From Table 1 it is known that the matrix consists of a one phase ε-Co structure after homogenization and quenching and by analogy with the results of the Co-17Re-23Cr-15Ni alloy it can be derived that the first three peaks demonstrate a combined process of σ phase and fcc phase formation. Figure 8c shows that only a small amount of σ phase has formed by reaching a temperature of 1 040 °C. Nevertheless, the peak amplitude is comparable to those of the alloys with 23 at.% Cr in which more σ phase has formed. But the thermodynamic calculations of the alloys with 18 at.% Cr (see Fig. 10a and b) reveal that a significant amount of σ phase has formed in the

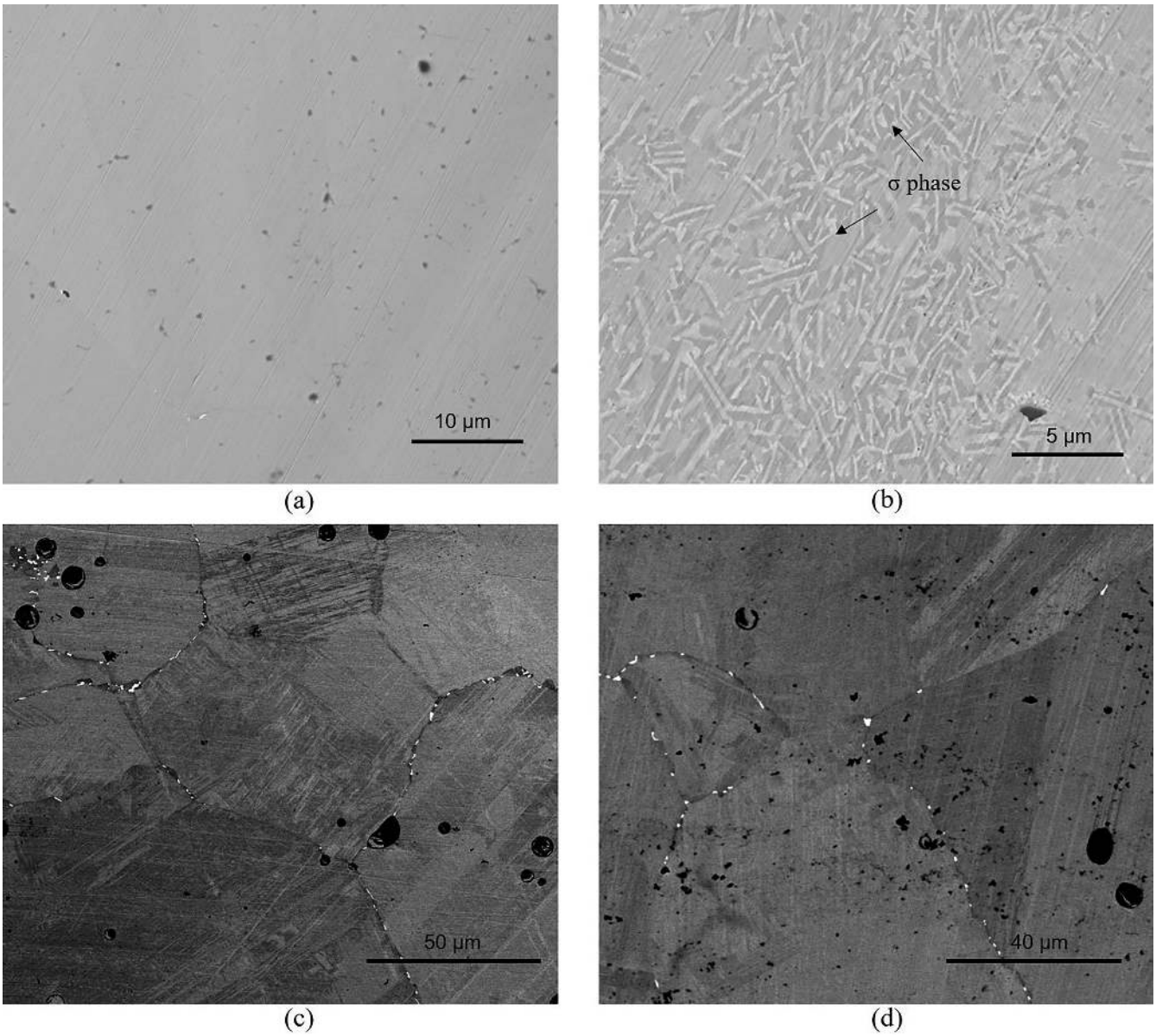

Fig. 9. SEM images obtained by the BSE detector of the alloy Co-17Re-18Cr-25Ni heated up to (a) 900 °C (area without evidence of σ), (b) 900 °C (area exhibiting σ), (c) 1 100 °C, and (d) 1 200 °C.

steady state condition at 1 000 °C. So it can be concluded due to decelerated kinetics that this steady state condition is achieved at a higher temperature in the DSC heating curve causing the 1 056 °C peak. The appearance of the next peak at 1 132 °C is different as compared to that shown in Fig. 4a. The SEM micrograph of the sample heated up to 1 300 °C (see Fig. 8d) shows a homogeneous matrix without σ particles. Thermodynamic calculations of the volume fractions of the different phases as a function of the temperature (see Fig. 10a) reveal that the σ phase has dissolved by reaching a temperature of 1 200 °C. So it can be concluded that this signal belongs to the σ phase dissolution. Another endothermic signal appears at 1 260 °C. As the σ phase has already dissolved, this signal can only be related to the fcc formation. This conclusion corresponds to the results of the thermodynamic calculations in which the fcc phase fraction is increased at 1 200 °C (see Fig. 10a).

The alloy Co-17Re-18Cr-25Ni exhibits a DSC curve similar to the one of Co-17Re-18Cr-15Ni, but the peak at 1 260 °C does not form. The peak at 892 °C is similar to the first peak in the heating curves of the other alloys. The SEM micrographs of the additional sample (heated up to 900 °C) in Fig. 9a and b show some grains with nearly no σ phase and some areas where some σ phase precipitated. As the thermodynamic calculations in Fig. 10b predict a two-phase ε+γ matrix phase with an increasing fcc volume fraction over the whole temperature range it is assumed that the σ phase formation is also combined with the $\varepsilon \rightarrow \gamma$ transformation in the alloys with 18 at.% Cr. The BSE micrographs of the additional samples heated up to 1 100 and 1 200 °C (Fig. 9c and d) reveal that the dissolution of the σ phase takes place at these temperatures as the volume fraction of the σ phase is strongly decreased in comparison to Fig. 9b. This experimental observation is in accordance to the thermodynamic calculations in which the σ phase has dissolved at 1 200 °C. So, the three consecutive peaks can be accounted for as the σ phase formation and dissolution and the simultaneous $\varepsilon \rightarrow \gamma$ transformation.

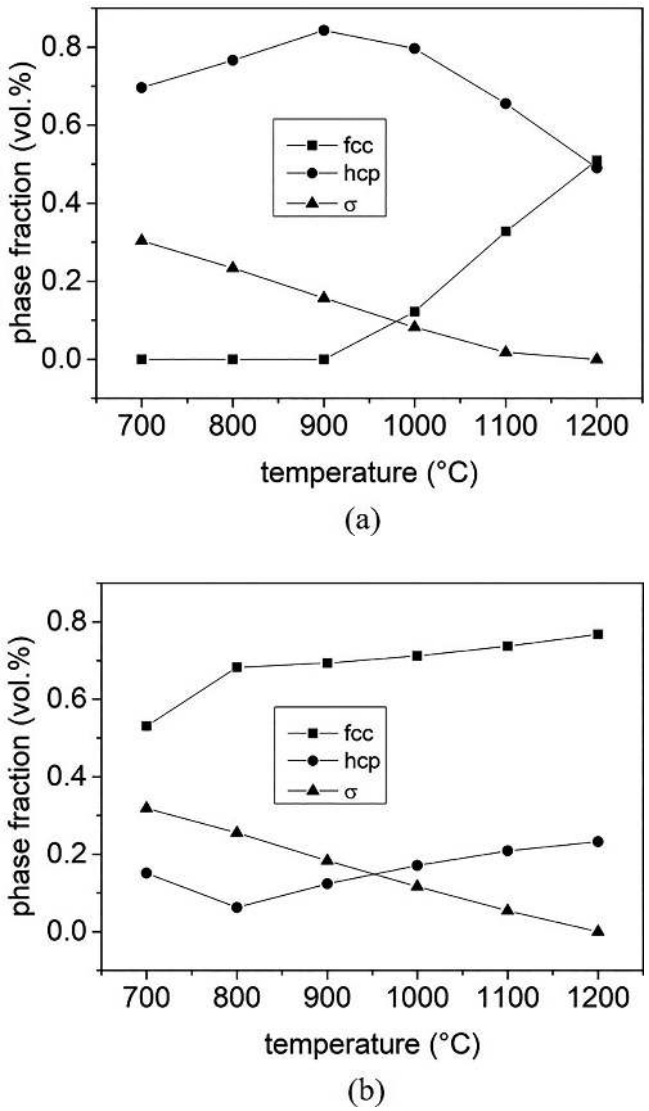

Fig. 10. Thermodynamic calculations of the phase fractions of the different phases in the temperature range of 700–1 200 °C in alloy (a) Co-17Re-18Cr-15Ni, and (b) Co-17Re-18Cr-25Ni using the software FactSage.

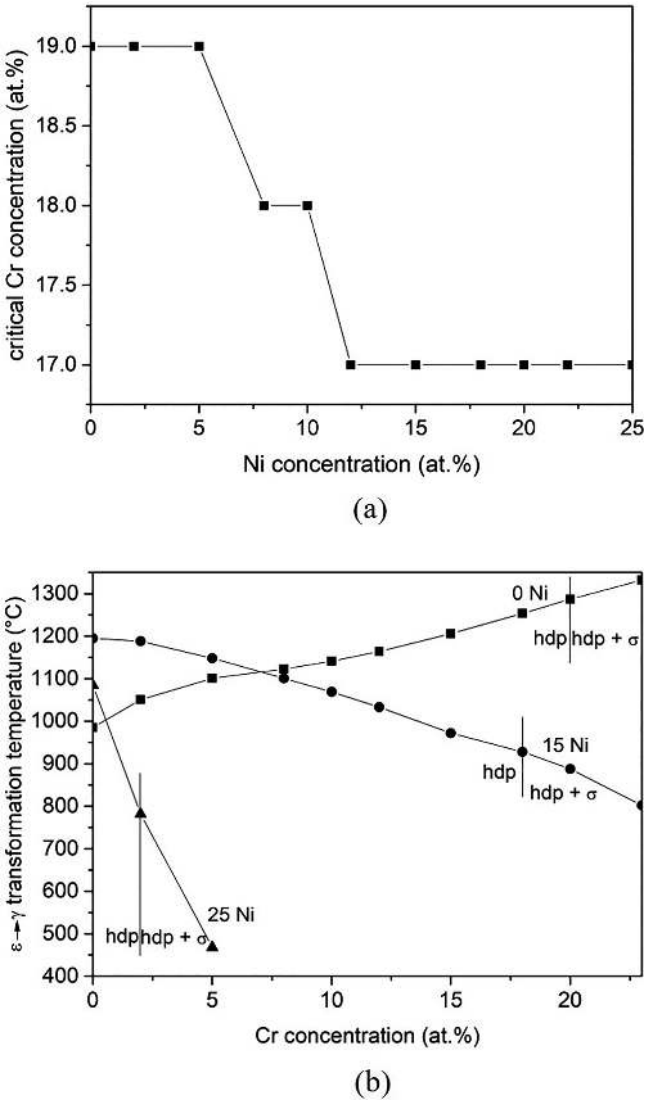

Fig. 11. Thermodynamic calculations using the software FactSage: (a) critical Cr concentration for σ phase formation at 1 000 °C in the alloy system Co-17Re-*X*Cr-*Y*Ni, and (b) Cr effect on the ε → γ transformation temperature of the alloy system Co-17Re-*X*Cr-*Y*Ni ($Y = 0, 15, 25$).

The experiments reveal that all investigated alloys exhibit the formation of the σ phase during high-temperature exposure, but the solvus temperature of the σ phase depends on the Cr concentration of the alloy. The experimental investigations showed that the σ phase in the Co-17Re-18Cr-XNi alloys dissolves at temperatures of 1 100 – 1 200 °C, whereas the alloys with 23 at.% Cr exhibit higher temperature stability of the σ phase (see Figs. 4d and 7).

Combined effect of Ni and Cr

The results presented above clearly show that Cr primarily governs the formation of the σ phase. The comparison of the microstructures of alloys with 18 at.% and 23 at.% Cr reveals that the volume fraction of the σ phase dramatically enhances with increasing Cr content (see Figs. 4, 8 and 9). Regarding the σ phase stability, Ni seems to have a significant effect, too. Peckner and Bernstein [30] stated that in austenitic stainless steels with a chromium concentration below 20 wt.%, the precipitation of the σ phase is not readily observed. Thermodynamic calculations performed by Gorr et al. [31] predicted that a Cr concentration of 20 at.% is required for the existence of the σ phase at 1 000 °C in the Co-17Re-Cr system. However, the experimental results in this study show that the Ni-containing Co-17Re-18Cr alloys contain σ phase precipitates although their Cr concentration is lower than 20 at.%. Based on the results shown above, it seems that Ni reduces the critical Cr content which is required for the formation of the σ phase. This assumption is confirmed by the results of further thermodynamic calculations. Figure 11a shows the critical Cr concentration needed for the formation of the σ phase at 1 000 °C, as a function of the Ni content in the alloy system Co-17Re-*X*Cr-*Y*Ni. It becomes clear that with increasing Ni content less Cr is required for the occurrence of the σ phase at 1 000 °C. If the Ni concentration exceeds about 8 at.%, the critical Cr concentration for σ phase formation is slightly decreased. The step-like progression is attributed to

the formation and composition character of the σ phase as well as to the calculation steps.

As discussed above, Ni clearly stabilizes the fcc phase. Apparently, Cr also seems to influence the matrix in Co–Re–Cr–Ni alloys. Regarding the $\varepsilon \leftrightarrow \gamma$ transformation, Cr acts as an hcp stabilizer which increases the transformation temperature [32]. However, thermodynamic calculations reveal that the Cr effect on the $\varepsilon \leftrightarrow \gamma$ transformation changes if the matrix additionally contains Ni. Figure 11b shows the calculated $\varepsilon \rightarrow \gamma$ transformation temperatures as a function of the Cr concentration of Ni-free and Ni-containing Co-17Re-*X*Cr alloys. While the Ni-free alloy system exhibits an increasing transformation temperature with a higher Cr content, the Ni-containing alloy systems show that the temperature of allotropic transformation is lowered with increasing Cr concentration. The more Ni in the alloy, the stronger is the decreasing effect on the transformation temperature. The black vertical lines in Fig. 11b mark the concentration boundaries between the single-phase hcp region and the two-phase hcp + σ field. The smooth course of the transformation temperature vs. Cr concentration curves does not seem to be affected by the intercept of the phase boundary hcp/hcp + σ. This indicates that the Cr effect on the hcp stability is pervasive for this alloy system, i. e. the effect is independent of the fact whether the σ phase is present in the alloy or not. The temperature curve of the alloy system with 25 at.% Ni ends at 5 at.% Cr as with higher Cr concentration the fcc phase is already stable at room temperature. This trend is also visible in the experimental results of the solution annealed state as both alloys with 25 at.% Ni contain fcc phase (see Table 1).

In conclusion, the effects of Ni and Cr on the microstructure of the Co–Re–Cr–Ni alloys can be summarized as followed. Ni has two strong effects: (i) it stabilizes the fcc phase as the $\varepsilon \leftrightarrow \gamma$ transformation shifts to lower temperatures, and (ii) Ni reduces the Cr concentration required for the σ phase formation.

Cr has a significant effect on the alloy microstructure as well. Firstly, Cr, in addition to Ni, stabilizes the fcc phase (if Ni is also present in the alloy) as the $\varepsilon \leftrightarrow \gamma$ transformation temperature decreases with the Cr content. Secondly, the solvus temperature of the σ phase increases with an enhanced Cr concentration.

It should be pointed out that some results of the thermodynamic calculations do not perfectly correspond to the experimental results. For example, the σ phase in Co-17Re-18Cr-15Ni is not stable at 1 200 °C according to the thermodynamic calculations although the DSC measurements indicate the dissolution of the σ phase with a peak temperature of 1 260 °C. Such differences can clearly be attributed to the kinetic effect as thermodynamic predictions relate to the phases in thermodynamic equilibrium.

4. Conclusions

The microstructural evolution of four Co–Re–Cr–Ni alloys with different Cr and Ni concentrations was investigated during high-temperature exposure. Based on various experimental results and assisted by thermodynamic calculations, the effect of Cr and Ni on the microstructure could be identified. It was found that the alloys with a Cr content of 18 at.% exhibit a lower volume fraction of the σ phase compared to those with 23 at.%. While Cr increases the solvus temperature of the σ phase, Ni decreases the concentration of Cr required for the formation of the σ phase. The volume fraction of the fcc phase clearly increases with increasing Ni concentration. The fcc phase seems to be additionally stabilized by Cr particularly in Ni-containing Co–Re–Cr alloys.

Part of this work was performed at the Micro- and Nanoanalytics Facility (MNaF) of the University of Siegen. The authors thank Heinz Maier-Leibnitz Zentrum (FRM II) for providing beam time.

References

[1] A. Mottura, R.C. Reed: MATEC Web Conf. 14 (2014). DOI:10.1051/matecconf/20141401001
[2] D.L. Anton, F.D. Lemkey, in: M. Gell, C.S. Kortovich, R.H. Bricknell, W.B. Kent, J.F. Radavich (Eds.), Superalloys 1984, The Minerals, Metals & Materials Society, Warrendale, PA (1984) 601.
[3] A.F. Giamei, D.L. Anton: Metall. Trans. A, 16 (1985) 1997. DOI:10.1007/BF02662400
[4] W.S. Walston, J.C. Schaeffer, W.H. Murphy: Superalloys 1996 (1996) 9. DOI:10.7449/1996/Superalloys_1996_9_18
[5] R. Darolia, D.F. Lahrmann, R.D. Field: Superalloys 1988 (1988) 255. DOI:10.7449/1988/Superalloys_1988_255_264
[6] J. Rösler, D. Mukherji, T. Baranski: Adv. Eng. Mater. 9 – 10 (2007) 876. DOI:10.1002/adem.200700132
[7] D. Mukherji, J. Rösler, P. Strunz, S. Piegert: Int. J. Mater. Res. 102 – 9 (2011) 1125. DOI:10.3139/146.110563
[8] M. Heilmaier, J. Rösler, D. Mukherji, M. Krüger in Microstructural Design of Advanced Engineering Materials, D.A. Molodov (eds.), Wiley-VCH, (2013). DOI:10.1002/9783527652815.ch19
[9] B. Gorr, V. Trindade, S. Burk, H.-J. Christ, M. Klauke, D. Mukherji, J. Rösler: Oxid. Met. 71 (2009) 157. DOI:10.1007/s11085-008-9133-y
[10] M. Heilmaier, M. Krüger, H. Saage, J. Rösler, D. Mukherji, U. Glatzel, R. Völkl, R. Hüttner, G. Eggeler, Ch. Somsen, T. Depka, H.-J. Christ, B. Gorr, S. Burk: JOM-J. Min. Met. Mat. S. 61 (2009) 61. DOI:10.1007/s11837-009-0106-7
[11] L. Wang, B. Gorr, H.-J. Christ, D. Mukherji, J. Rösler: Corros. Sci. 93 (2015) 19. DOI:10.1016/j.corsci.2015.01.004
[12] K. Esleben, B. Gorr, H.-J. Christ, D. Mukherji, J. Rösler: Mater. High Temp. 35 (2018) 177. DOI:10.1080/09603409.2017.1392111
[13] P. Beran, D. Mukherji, P. Strunz, R. Gilles, M. Hölzel, J. Rösler: Adv. Mater. Sci. Eng. 2018 (2018) 6. DOI:10.1155/2018/5410871
[14] K. Dörries, D. Mukherji, J. Rösler, K. Esleben, B. Gorr, H.-J. Christ: Metals 8 (2018) 706. DOI:10.3390/met8090706
[15] M. Hoelzel, A. Senyshyn, N. Juenke, H. Boysen, W. Schmahl, H. Fuess: Nucl. Instr. A 667 (2012) 32. DOI:10.1016/j.nima.2011.11.070
[16] J. Rodriguez-Carvajal: Physica B 192 (1993) 55. DOI:10.1016/0921-4526(93)90108-I
[17] I. Hatta, H. Ichikawa, M. Todoki: Thermochim. Acta 267 (1995) 83. DOI:10.1016/0040-6031(95)02468-9
[18] W.-R. Wang, W.-L. Wang, J.-W. Yeh: J. Alloys Compd. 589 (2014) 143. DOI:10.1016/j.jallcom.2013.11.084
[19] M. Palumbo, T. Abe, C. Kocer, H. Murakami, H. Onodera: CALPHAD 34 (2010) 495. DOI:10.1016/j.calphad.2010.09.003
[20] Y. Dong, L. Jiang, Y. Lu, T. Wang, T. Li: Mater. Design, 82 (2015) 91. DOI:10.1016/j.matdes.2015.05.046
[21] Y. Liu, H. Yang, Y. Liu, B. Jiang, J. Ding, R. Woodward: Acta Mater. 53 (2005) 3625. DOI:10.1016/j.actamat.2005.04.019
[22] B. Milkereit, N. Wanderka, C. Schick, O. Kessler: Mat. Sci. Eng A-Struct. 550 (2012) 87. DOI:10.1016/j.msea.2012.04.033
[23] J.W. Christian: P. Roy. Soc. A-Math. Phy. 206 (1951) 51. DOI:10.1098/rspa.1951.0055
[24] C.M. Garzón, A.J. Ramirez: Acta Mater. 54 (2006) 3321. DOI:10.1016/j.actamat.2006.03.018
[25] E. Baerlecken, H. Fabritius: Arch. Eisenhuttenwes. 26 (1955) 679. DOI:10.1002/srin.195502095
[26] C-C. Hsieh, W. Wu: ISRN Metallurgy 2012 (2012). DOI:10.5402/2012/732471
[27] R.J. Gray, V.K. Sikka, R.T. King: JOM-J. Min. Met. Mat. S. 30 (1978) 18. DOI:10.1007/BF03354388
[28] D. Mukherji, J. Rösler, J. Wehrs, P. Strunz, P. Beran, R. Gilles, M. Hofmann, M. Hölzel, H. Eckerlebe, L. Szentmiklosi, Z. Macsik: Metall. Mater. Trans. A 44 (2013) 1834. DOI:10.1007/s11661-012-1363-6

[29] D. Mukherji, P. Strunz, R. Gilles, L. Karge, J. Rösler: Kovove Mater. 53 (2015) 287. DOI:10.4149/km-2015-4-287
[30] D. Peckner, I.M. Bernstein: Handbook of Stainless Steels, McGraw-Hill, New York, (1977).
[31] B. Gorr, H.-J. Christ, D. Mukherji, J. Rösler: J. Alloys Compd. 582 (2014) 50. DOI:10.1016/j.jallcom.2013.07.055
[32] D. Mukherji, P. Strunz, S. Piegert, R. Gilles, M. Hofmann, M. Hölzel, J. Rösler: Metall. Mater. Trans. A 43 - 6 (2012) 1834. DOI:10.1007/s11661-011-1058-4

(Received May 14, 2019; accepted August 13, 2019)

Correspondence address

Katharina Esleben M. Sc.
Institut für Werkstofftechnik
University of Siegen
Paul-Bonatz-Straße 9 – 11
D-57068 Siegen
Germany
Tel: +49 271 740 4660
Fax: +49 271 740 2545
E-mail: Katharina.esleben@uni-siegen.de

Bibliography
DOI 10.3139/146.111855
Int. J. Mater. Res. (formerly Z. Metallkd.)
110 (2019) 12; page 1092 – 1104

ISSN 1862-5282